

Random and oriented electrospun fibers based on a multicomponent, in situ clickable elastin-like recombinamer system for dermal tissue engineering

Israel González de Torre¹, Arturo Ibáñez-Fonseca¹, Luis Quintanilla¹, Matilde Alonso¹, José-Carlos Rodríguez-Cabello¹

¹ BIOFORGE, CIBER-BBN, Edificio Lucia, Universidad de Valladolid, Paseo Belén 19, 47011, Valladolid, Spain.

Dr. Israel Gonzalez de Torre
G.I.R BIOFORGE, Universidad de Valladolid
Paseo de Belen 19
47011, Valladolid, Spain
E-mail: igonzalez@bioforge.uva.es

Dr. Arturo Ibáñez-Fonseca
G.I.R BIOFORGE, Universidad de Valladolid
Paseo de Belen 19
47011, Valladolid, Spain
E-mail: aibanez@bioforge.uva.es

Prof. Luis Quintanilla
G.I.R BIOFORGE, Universidad de Valladolid
Paseo de Belen 19
47011, Valladolid, Spain
E-mail: luisq@ele.uva.es

Prof. Matilde Alonso
G.I.R BIOFORGE, Universidad de Valladolid
Paseo de Belen 19
47011, Valladolid, Spain
E-mail: malonso@bioforge.uva.es

Prof. José Carlos Rodríguez Cabello
G.I.R BIOFORGE, Universidad de Valladolid
Paseo de Belén 19
47011, Valladolid, Spain
E-mail: roca@bioforge.uva.es

Keywords: electrospun fibers, elastin-like recombinamers, click reaction, wound healing.

ABSTRACT

Herein we present a system to obtain fibers from clickable elastin-like recombinamers (ELRs) that crosslink *in situ* during the electrospinning process itself, with no need for any further treatment to stabilize them. These ELR-click fibers are completely stable under *in vitro* conditions. A wrinkled fiber morphology is obtained. In addition to a random fiber orientation, oriented fibers with a high degree of alignment and coherence can also be obtained by using a rotational electrode. The production of multicomponent fibers means that different functionalities, such as cell-adhesion domains (RGD peptides), can be incorporated into them. In a subsequent study, two main cell lines present in the dermis and epidermis, namely keratinocytes and fibroblasts, were cultured on top of the ELR-click fibers. Adhesion, proliferation, fluorescence, immunostaining and histology studies showed the cytocompatibility of these scaffolds, thus suggesting their possible use for wound dressings in skin tissue engineering applications.

1. INTRODUCTION

Novel biomaterials and biomanufacturing methods aimed at the development of scaffolds for different tissue-engineering applications have been designed and tested in recent years [1-6]. Indeed, several constructs have been produced and used for the regeneration of different tissues, such as nerves [7, 8], tendons [9, 10], muscles, bones [11-14] and skin [15-17]. The latter is the largest organ in the body and the main barrier isolating it from the surrounding environment, thereby protecting it against external aggressions, including bacterial infections and chemical or physical damage [18]. The epidermis and dermis, which are outermost layers of the skin, are mainly composed of keratinocytes and fibroblasts, respectively [19], and the presence of elastin is crucial to maintain the mechanical properties and elasticity of these tissues [20]. The onset of a wound-healing process after trauma or skin damage leads to a scar tissue that gradually restores the skin barrier over a period of days, weeks or even months, depending on the severity of the damage [21]. However, the structure of this new skin is not the same as the original. For instance, this scar tissue lacks the elasticity of the original skin, and the higher collagen production during the wound-healing process leads to a tissue that is stiffer than its natural counterpart [22]. Hence, it is of great interest to manufacture elastin-based constructs for use in skin tissue engineering.

The different techniques used to develop scaffolds for this purpose include electrospinning, which involves the formation of fibers by application of a high voltage to a polymer solution expelled through a syringe to create a charged liquid jet that flies until it reaches a collector, where the fibers are formed [23-25]. The liquid dries during this flight, thus allowing the polymer to assemble into a fiber if its properties have been adjusted appropriately. However, in most cases biopolymer-based fibers need to be cross-linked with chemical reagents in order to avoid dissolution of the polymer when immersed in water-based solvents or when used in tissue engineering [24, 26, 27]. Furthermore, electrospinning allows the formation of random or axially aligned fibers, for example by incorporating a mechanically rotating collector into the system [8, 28-30].

Although obtained using a complex and not always feasible set-up, these aligned fibers may find uses in the regeneration of different tissues that require cell alignment for optimal healing, such as tendon or nerve tissue [4, 31]. However, other tissues, including skin, do not contain aligned structures and the collagen and elastin fibers present in the extracellular matrix are randomly oriented [32-35]. As such, fiber-based constructs designed for skin regeneration do not necessarily have to be micro- or macroscopically oriented.

With regard to the mechanical properties of electrospun fibers, several materials can be used to optimize the elasticity, with most of these being synthetic polymers whose biocompatibility can be compromised by their nature [27]. Nevertheless, new recombinant biomaterials with potential applications in tissue engineering have arisen in the last decades [36], thus facilitating the development of tailored protein-based biopolymers. One of the most exciting recombinant biomaterials are the so-called elastin-like recombinamers (ELRs) [37], which are formed by repetitive units of the Val-Pro-Gly-X-Gly (VPGXG)_n peptide, in which X (guest residue) can be any amino acid except L-proline [38]. This pentapeptide exhibits an inherent elasticity as it fold into a β -turn above the so-called transition temperature (T_i) [39]. One of the main characteristics of the ELRs is their inherent change of structure in water solution depending on the temperature (transition temperature, T_t), which means that below the T_t the ELR remains soluble, and above this T_t the ELR excludes water and precipitates [36-39]. Furthermore, the possibility of using amino acids containing reactive groups in their side chains as guest residues, such as L-lysine, means that they can be modified to include groups that are even more reactive in order to achieve a “click” chemistry reaction between ELR molecules [40, 41], thereby simulating the physiological covalent cross-linking of tropoelastin mediated by lysyl oxidases [42, 43]. Although this approach can also be adapted for the formation of *in situ* cross-linked electrospun fibers, to the best of our knowledge there are no reports in the literature in this regard. Hence, in this work, and for the first time, we provide evidence for the formation of ELR-based fibers that are cross-linked *in situ* using an orthogonal “click” reaction between azide and cyclooctyne groups present in two different ELR molecules, as reported previously [40, 41, 44, 45], without the need for further crosslinking or post-treatment steps.

The recombinant DNA technology used for the biosynthesis of ELRs also allows the inclusion of bioactive peptides or proteins that may improve the biocompatibility of this type of biomaterials, such as cell adhesion domains comprising the tri-peptide Arg-Gly-Asp (RGD) [46]. It should be noted that hydrogels formed by the cross-linking of RGD-containing ELRs following the aforementioned “click” methodology have recently been shown to be cyto- and biocompatible using several methods [47], thereby anticipating the good biocompatibility of ELR-based “clickable” electrospun fibers.

In this work stable, electrospun bioactive fibers are obtained by the *in situ* mixing of two “clickable” ELR components during the flight of the ELR solutions from the needle of the syringe to the collector. Both random and oriented fibers are achieved after optimization of the electrospinning parameters. Moreover, these bioactive fibers

are able to support cell growth due to the inclusion of RGD motifs. Finally, *in vitro* biocompatibility is tested using the two main cell types found in the outer layers of skin, namely fibroblasts and keratinocytes. Herein, we present the results from electrospinning optimization, fiber size and orientation, cell adhesion and proliferation, and general cell behavior (cell growth, migration and alignment) along ELR click fibers.

2. Materials and Methods

2.1. ELRs

The two ELRs used in this work were kindly provided by Technical Proteins NanoBiotechnology S.L. (TP70904, TP20254, respectively). One of them is a structural polymer with 60% of the amines from the lysine residues functionalized with cyclooctyne groups (VKVx24-cyclo), whereas the second one comprises integrin-mediated cell adhesion domains, namely the L-Arginine-Glycine-L-Aspartic acid tripeptide (RGD), functionalized to the same degree as the former but in this case to include azide groups in the lysines present in the ELR (HRGD6-N₃).

The sequences of the ELRs are:

VKVx24: MESLLPVGVPGVG-[VPGKG-(VPGVG)₅]₂₃-VPGKG-(VPGVG)₃-VPGV

HRGD6: MGSSHHHHHSSGLVPRGSHMESLLP-[[$(\text{VPGIG})_2$ -VPGKG- $(\text{VPGIG})_2$]₂]-AVTGRGDSPASS-
[[$(\text{VPGIG})_2$ -VPGKG- $(\text{VPGIG})_2$]₂]₆-V.

A detailed explanation of the ELRs synthesis and the characterization of multicomponent click hydrogels implemented with these ELRs have been previously reported [41].

2.2. ELR-click fiber formation

All electrospinning experiments were conducted using a syringe infusion pump (PHD 2000 Harvard apparatus) and a high voltage DC power supply (Glassman high voltage inc. FC series). HRGD6-N₃ and VKVx24-cyclo were dissolved in 2,2,2-trifluoroethanol (TFE) (Sigma-Aldrich) at a concentration of 50 mg/mL at room temperature. Recombinamer solutions were placed in 1 mL Hilton syringes (Luer Lock) connected by a specially designed mixing tip with a 23G needle. Fibers were collected on glass cover slips placed over a copper collector.

Aligned samples were obtained using a rotary mandrel at a fixed surface speed. This mandrel comprised a copper parallelepiped attached to a shaft, which is inserted into a motor (IKA Eurostar 20 digital). Aligned fibers were collected on coverslips placed on alternating sides of the copper parallelepiped (Fig. 1).

All the fibers obtained were incubated in water at 277 K for at least 12 hours to assess the covalent crosslinking and stability of the fibers.

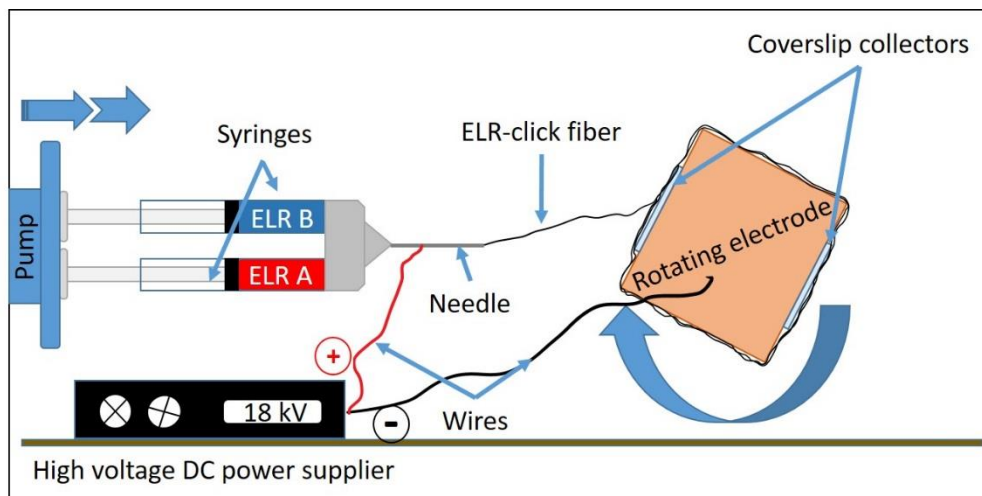


Fig. 1. Schematic set-up of the rotating electrospinning device.

2.3. Scanning electron microscopy

Scanning electron microscopy (SEM) was used to investigate the fiber morphology. Thus, ELR-click fibers were immersed in cold water (277K) for at least 12 h. Finally, samples were dried at 313 K for 24 h. Images of the ELR-click fibers were obtained by SEM (JEOL, JSM-820) with no prior coating procedures. Some of the SEM images were colored using Jasc Paint Shop Pro 9 software (Corel).

2.4. Evaluation of fibers dimensions and orientation

Cell and fiber orientation was evaluated using the OrientationJ plug-in of the FIJI-Image J software, as described by Puspoki *et al.* and others [48-50]. Coherency was evaluated for each pixel of an input image by computing the continuous spatial derivatives and using a cubic spline interpolation [51]. Fiber diameters were determined using the Diameter J plug-in of the FIJI-Image J software. Raw numerical data were processed and analyzed using the

SigmaPlot 12.0 software or Excel 2016 from Microsoft. Randomly chosen regions of nine different samples were analyzed.

2.5. Mechanical properties of the scaffolds: micro-tensile test

Tensile strength tests were performed using a precision instrument for small-scale testing (Instron 5944 MicroTester). Ten 30 mm x 5 mm specimens were clamped using anti-slip clamps leaving a gap of 10 mm between the clamps. Tests were performed at 2 mm/s. Load-deformation data were recorded and the stress-strain curve (Fig. 6 SI) of the fibrous structure was obtained from the load-deformation data.

2.6. Contact angle

In order to measure the hydrophobicity of the sample, contact angle measurements were carried out at 295 K using the sessile drop method and a Data Physics OCA20 system instrument. The drop profile images during micro-syringe dispensation of ultra-pure water (mQ) were recorded using an adapted CCD video camera. Contact angles were measured on both sides of the drop and the average values are reported. The stainless-steel needle tip was maintained at the top of the sessile drop, and immersion of the needle into the drop was avoided during the measurements to prevent distortion of the drop shape by the needle. Fifteen measurements from different samples with oriented and random fibers were obtained to ensure a representative value for the contact angle.

2.7. Cell culture

Basal medium Dulbecco's modified Eagle's medium (DMEM, ref 31966-021), fetal bovine serum (FBS ref. 16000-044), penicillin streptomycin solution (ref. SV30010), trypsin-EDTA (ref. SV30010), DPBS (ref 14190250, GIBCO), Trypan Blue stain 0.4% (ref. 15250061), Alexa Fluor 488 phalloidin (ref. A12379), DAPI (ref. D21490) were supplied by Invitrogen. Human foreskin fibroblasts HFF-1 (SCRC-1041) were purchased from the American Type Culture Collection (ATCC, USA). Immortalized keratinocytes (HaCaT cells) were kindly supplied by the Tissue Engineering and Regenerative Medicine Group (TERMeG) at the Universidad Carlos III de Madrid (UC3M), Spain. All cell culture plastic-ware and consumables were acquired from NUNC. HaCaT and HFF1 were cultured in DMEM supplemented with 100 U mL⁻¹ penicillin, 0.1 mg mL⁻¹ streptomycin and 10% FBS. Cells were incubated at 37 °C in a 10% CO₂ humidified environmental chamber and the medium was replaced every 2 days.

2.8. Cell adhesion and proliferation

A cell proliferation assay was performed using a double stranded DNA (dsDNA) quantification kit (Picogreen®, Invitrogen). Thus, HFF-1 (3000 cells/cm²) and HaCaT cells (3000 cells/cm²) were seeded separately on matrices of randomly aligned ELR-click fibers deposited on glass coverslips, which were placed in 24-well plates and subsequently treated with 1% BSA to avoid unspecific cell adhesion to the carrier. Next, cells were incubated for 4 h (adhesion test), and 1, 3 and 7 days (proliferation test). After culture, samples were washed twice with DPBS and 250 µL of ultra-pure water. The samples were frozen at 193 K until analysis. For DNA quantification, the samples were thawed and the freeze-thaw cycle was repeated twice to achieve cell lysis. The reagent, TE buffer and samples were added in triplicate to a 96-well opaque plate (Falcon). Fluorescence was measured using a microplate reader, with an excitation wavelength of 480 nm and an emission wavelength of 528 nm.

2.9. Cell behavior

HFF-1 (3000 cells/cm²) and HaCaT cells (3000 cells/cm²) were seeded separately on the randomly aligned ELR-click fibers and incubated for 48 h. Images were taken every 5 minutes using a CytoSmart Lux2 imaging system. Images were processed to obtain a movie using the Windows Moviemaker 2012 (Microsoft Corporation) software.

2.10. Cell staining

To stain cells for image acquisition, they were first fixed in 4% paraformaldehyde (Sigma-Aldrich, ref. P6148) for 15 min at room temperature (RT). Samples were then permeabilized with 0.1% Triton X-100 (Sigma-Aldrich, ref. T9284), blocked with 1% BSA (Sigma-Aldrich, ref. A9418), and actin was stained with Phalloidin-Alexa Fluor® 488 (Invitrogen, ref. A12379), using cells seeded on random and oriented fibers. As regards vinculin staining, samples of cells seeded on randomly aligned fibers were incubated with a mouse anti-vinculin solution (Sigma-Aldrich, ref. V9131; 1:400) for 1 h at RT. After subsequent washing, samples were then incubated with a secondary antibody solution (goat anti-mouse IgG H&L conjugated to Alexa Fluor® 568, Abcam, ref. ab175473; 1:400). Finally, cell nuclei from samples used for actin or vinculin labeling were stained with DAPI (Invitrogen, ref. D21490; 300 nM). Samples were then observed under an epifluorescence microscope (Nikon Eclipse Ti-E) coupled to a digital camera (Nikon DS-2MBWc). Images were obtained and processed using the NIS-Elements AR software (Nikon).

2.11. Histological staining

Samples for histology (cells seeded on randomly aligned fibers) were immersed in paraformaldehyde at 4% in PBS and stored at 277 K for 24 h, then washed in PBS and water. Hematoxylin-eosin staining was performed following well-established protocols. Briefly, the samples were dipped in hematoxylin stain for 30 seconds and rinsed in water for 1 minute. A 1% eosin solution was then used for staining during 30 seconds, with shaking, and samples were dehydrated by immersion in ethanol solutions (75%, 95% and 100%) with a final dehydration step in xylene (Sigma-Aldrich). Finally, mounting medium was used to cover the sample on the slide with a microscope coverslip. Images were captured using a bright field microscope (Nikon Eclipse 80i) coupled to a color camera (Nikon Digital Sight DS-Fi1) with different magnifications.

Elastin staining was performed by immersion in working elastic stain solution (20 mL hematoxylin, 3 mL of FeCl_3 , 8 mL of Weigert's iodine solution and 5 mL of ultrapure water) for 8 minutes. The samples were then twice washed with ultrapure water. A differentiation step was carried out by immersion in FeCl_3 for 4 minutes, followed by washing with tap water and EtOH (95%) and ultrapure water. Samples were then dipped in VAN GIESON solution for 2 minutes and dehydrated with EtOH 95%, EtOH 100% (5 min) and xylol (10 min). Finally, samples were covered with a coverslip for protection. Images were captured using a bright field microscope (Nikon Eclipse 80i) coupled to a color camera (Nikon Digital Sight DS-Fi1) with different magnifications.

2.12. Statistical analysis

Data are reported as mean \pm SD ($n = 3$). Statistical analysis was evaluated by one way analysis of variance using the Holm-Sidak method. A p value lower than 0.05 was considered to be statistically significant (** $p < 0.001$, * < 0.05 ; $p > 0.05$ indicates no significant differences, n.s.d.).

3. Results

3.1. Random fibers: parameter optimization, formation and characterization

Bicomponent electrospun fibers have been successfully produced by combining two different ELR solutions in TFE. Preliminary electrospinning experiments were performed to obtain the stable Taylor cone needed for the formation of uniform fibers. During these preliminary tests, several parameters, such as humidity, temperature, distance between electrodes, voltage and intensity, were adjusted to obtain homogeneous and stable fibers free from defects.

The final values obtained after optimization of these parameters and other environmental factors are reflected in Table 1 (first row).

FLOW RATE (mL/min)	VOLTAGE (kV)	DISTANCE (cm)	ELR (mg/mL)	CONC. STRUCTURE
0.005	18	9	50	Fibers
0.005	<18	9	50	Beads
0.005	>20	9	50	Broken fibers
0.005	18	>10	50	Beads and broken fibers
0.005	18	<8	50	Beads
<0.005	18	9	50	Spray
>0.005	18	9	50	Beads
0.005	18	9	<50	Spray

Table 1 Varied process conditions for the electrospinning process. First row corresponds to optimized parameters. All experiments were carried out at a temperature of 295-298 K and 30-35% of humidity

Structures other than fibers, ranging from electrospray to thin broken fibers with beads (Table 1), were obtained upon varying these parameters, as can be seen in Fig. 2. A continuous spray is produced below a concentration of 50 mg/mL, thus forming an amorphous layer, as can be seen in Fig. 2 A. Voltages higher than 20 kV and distances longer than 10 cm produce a mixture of beads and broken fibers, as can be seen in Fig. 2 C. In contrast, the optimal electrospinning parameters yield homogeneous and continuous fibers without almost no defects (Fig. 2 B and D). Higher deposition times yield denser matrixes with a higher number of fibers.

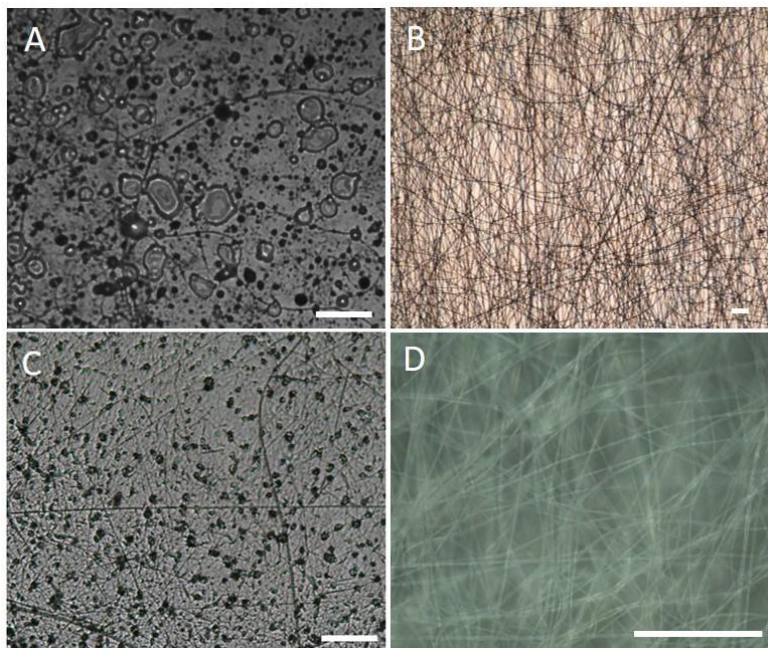


Fig. 2 Optical microscope images of several structures obtained after varying the electrospinning conditions. **A:** amorphous electrospayed layer (concentration and distance between electrodes: 25 mg/mL and 5 cm respectively). **B and D:** continuous ELR-click electrospun fibers (parameters shown in Table 1) and **C:** thin fibers and beads (applied voltage and distance between electrodes: 25 kV and 15 cm). Scale bars: 50 μm .

Crosslinking degree was evaluated by FTIR (see supporting info section). In agreement with reports in the literature [41], in our IR spectra, the azide band ($\sim 2100\text{ cm}^{-1}$) appears only at low percentage ($\sim 10\%$), thus indicating a high yield of the cross-linking reaction (around 90%). To corroborate the stability and cross-linked nature of the fibers, all samples were maintained in cold water (277 K) for at least 12 hours to dissolve non-crosslinked samples and leave only cross-linked fibers.

Scanning electron microscopy images (Fig. 3) showed a slight variation of the typical ribbon morphology for the fibers observed in other studies with electrospun elastin-based materials [52-54]. Our fibers seem to blend and to have longitudinal clefts. Thickness calculations performed using the DiameterJ plug-in from FIJI software gave an average fiber width of $1.11 \pm 0.45\ \mu\text{m}$. (Fig. 3 D).

In order to investigate the tensile properties of the electrospun scaffolds, microtensile tests were performed. Fig. 6 SI shows the strain–stress curves of scaffolds obtained after 300 s of electrospinning. An average tensile strength at failure value of $0.59 \pm 0.08\ \text{MPa}$ after a maximum percentage of strain of $247.5 \pm 36.08\%$, with a mean Young modulus of $1.73 \pm 0.95\ \text{MPa}$, was obtained.

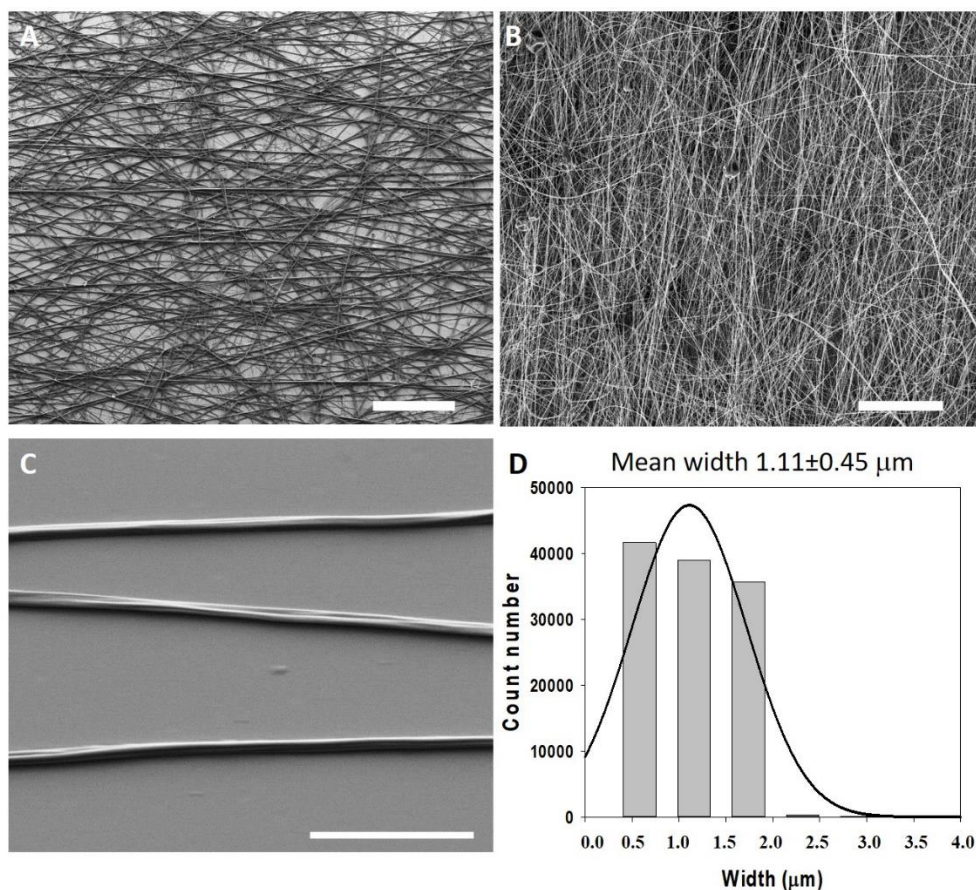


Fig. 3. Morphology and dimensions of ELR-click fibers. **A** (deposition time=90 s), **B** (deposition time=300 s) and **C** (deposition time=90 s): SEM micrographs of ELR-click fibers at different magnifications. Scale bars: **A** and **B** 100 μm , **C**: 10 μm . **D.** Statistical distribution of the fiber widths was obtained using the DiameterJ plug-in of Fiji (ImageJ). Fitting to a Gaussian distribution (continuous line) gave a mean width of $1.11 \pm 0.45 \mu\text{m}$.

3.2 Oriented fibers: formation and characterization

Further optimization of the parameters previously used to fabricate randomly oriented ELR-click fibers was performed in order to obtain oriented fibers. Aligned fibers were obtained after a careful tuning of the rotational speed applied to a rotatory mandrel. A speed of 1.8 m/s at the mandrel surface was fixed, and fibers were collected on two coverslips placed on the parallel, opposite faces of the collector (Fig. 1). A slower rotational speed than the optimum value yielded unaligned fibers, and velocities higher than 2.0 m/s yielded thin and broken fibers (data not shown).

A coherency of 83% in fiber orientation was found after analysis of the processed optical microscope and SEM images for the aligned fibers (Fig. 4). Fibers were oriented following the rotation direction of the mandrel. The experimental values of the angles were fitted according to a Gaussian distribution, giving a mean of 94.9° and

standard deviation of 8.1° , as can be seen in Fig. 4 C. Thus, fibers aligned with angles of between 80° and 120° were mainly obtained. Fig. 4 B represents a color survey after analysis using the OrientationJ plug-in, with the colors showing the coherency between oriented fibers. A red color is clearly predominant in the picture, thus meaning that the majority of the fibers are oriented in the same direction.

Contact angle measurements were carried out for deposition times longer than 90 s to evaluate the hydrophobicity of the scaffolds (Fig. 4 D). Samples with different fiber densities and alignments (random and oriented fibers) were analyzed, thus suggesting an increase in the hydrophobicity of the samples with deposition time, which corresponds to higher fiber densities. Measurements for a given deposition time include fibers with both types of alignment, since no significant difference was found between random and oriented fibers regarding the contact angle. Contact angles of $104.6 \pm 4.1^\circ$ were found for high-density samples (deposition times longer than 300 seconds), thus indicating a very highly hydrophobic scaffold. Even in the case of less dense samples, clearly significant differences ($p < 0.001$) were found in the values of the angles ($89.0 \pm 4.4^\circ$) with respect to the angles found on the coverslips used as collectors ($79.7 \pm 3.6^\circ$).

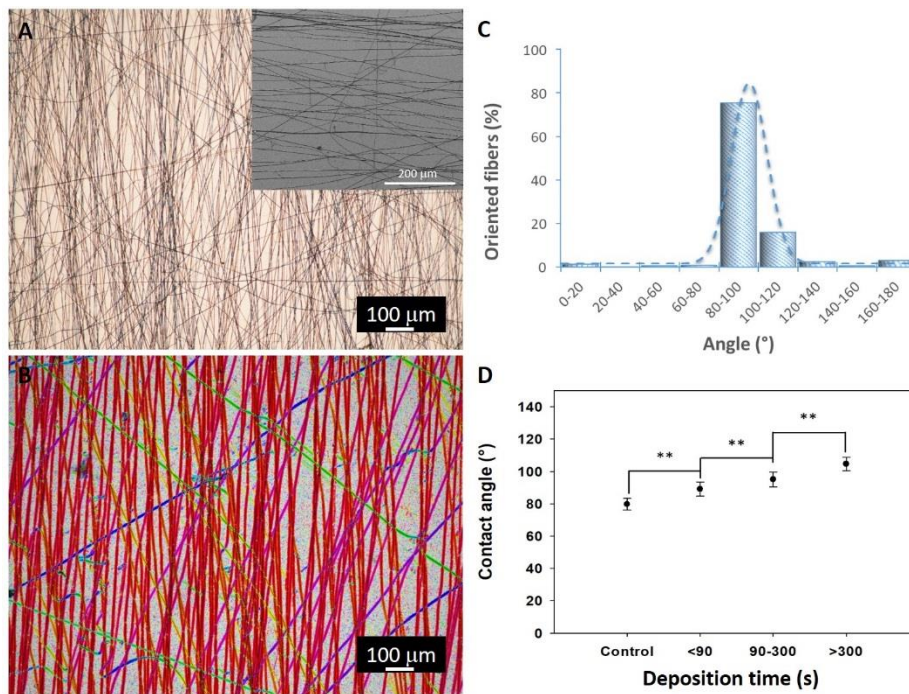


Fig. 4 Optical and SEM (insert) images of oriented ELR-click fibers (A). Color survey showing the directionality of the ELR-click fibers (B). Distribution of fiber orientation, data obtained using FIJI software. The dashed line corresponds to a Gaussian fitting of the experimental data (C). Contact angle values from hydrophobicity tests in samples with different fiber densities (samples with aligned and random fibers were analyzed) (D). Data are reported as mean \pm SD (n = 15). Statistical analysis was evaluated by analysis of variance using the Holm–Sidak method. **p < 0.001.

3.3 Dermal cell culture

3.3.1 Adhesion

The viability of typical cell lines found in skin, such as fibroblasts and keratinocytes, has been evaluated *in vitro*. In order to evaluate the cytocompatibility of the ELR-click fibers, human foreskin fibroblasts (HFF-1) and HaCaT keratinocytes were seeded on top of fiber mats. DNA was quantified after 4 hours for both cell lines in order to evaluate the number of cells adhered to the fibers in comparison with the positive and negative controls (TCP and BSA-blocked TCP, respectively). As can be seen from Fig. 5, both types of cells adhered to the fibers in a similar proportion to the positive control (n.s.d.), and far above the values obtained for the negative control (p < 0.001).

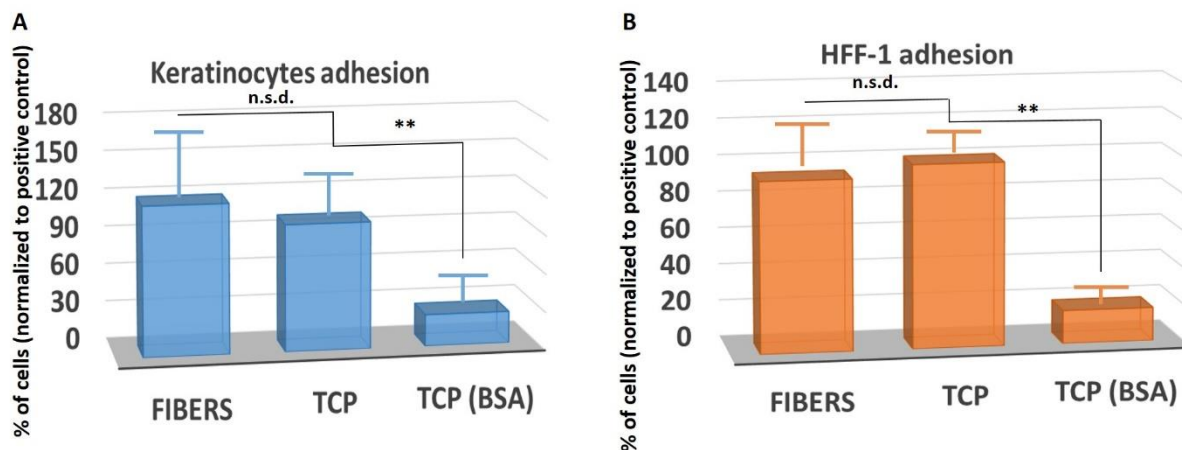


Fig. 5 Adhesion histograms for keratinocytes (HaCaT cells) (A) and fibroblasts (HFF-1) (B) after 4 hours of culture on ELR-click fibers (FIBERS), positive control (TP) and negative control (TCP(BSA)). Data are reported as mean \pm SD (n = 3). Statistical analysis was evaluated by performing an analysis of variance using the Holm–Sidak method. **p < 0.001; *p < 0.05; n.s.d., no significant differences.

3.3.2 Proliferation

In order to further assess the cytocompatibility of the aforementioned dermal cell lines, proliferation assays were performed by quantifying the DNA from cells seeded on ELR-click fiber mats and on the positive and negative controls at different time points, namely 1, 3 and 7 days. After one week, the cells on the positive controls reached

confluence, therefore this time-point was selected as the end of the experiment in order to compare the proliferation of these two cell lines on ELR-click fiber mats and controls (positive and negative). The results are depicted in Fig. 6. HFF-1 proliferation showed no statistically significant differences between the samples and TCP at any of the three time points. In contrast, clear differences in cell proliferation were found between the samples and the negative controls (Fig. 6 B). A similar trend was observed in the case of HaCaT cells (Fig. 6 A), in which p values <0.05 were found after culture for three days. This difference gradually disappeared over the next four days, and no significant differences could be observed between positive controls and samples at the end of the experiment. The values obtained for the negative controls were far lower than for the positive controls and samples in every case.

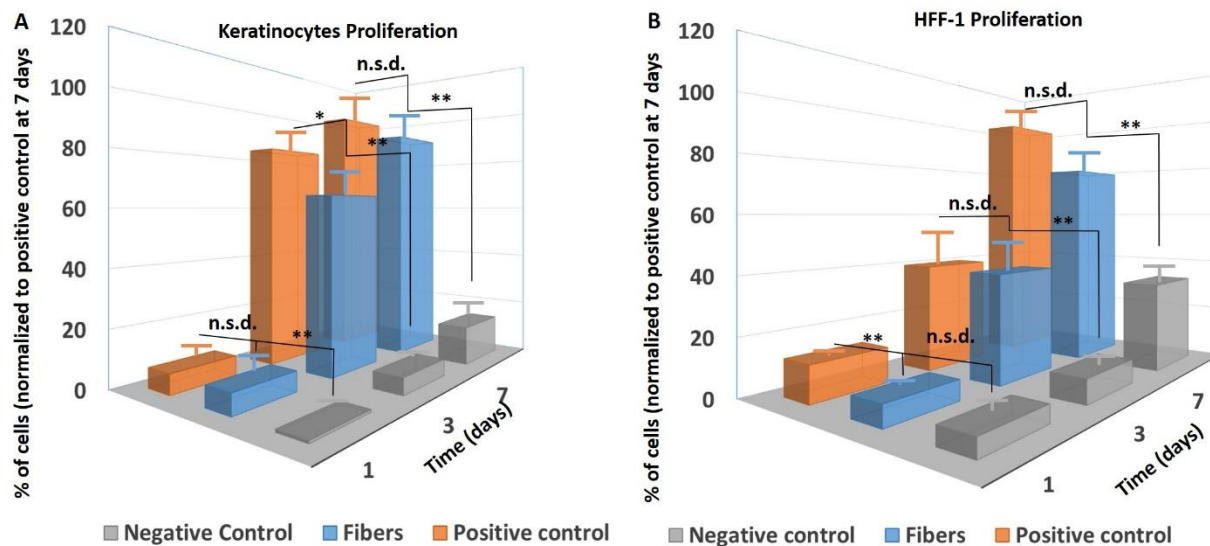


Fig. 6 Proliferation histograms of keratinocytes (HaCaT cells) (A) and fibroblasts (HFF-1) (B) after 1, 3 and 7 days of culture on ELR-click fibers (FIBERS), positive control (TP) and negative control (TCP(BSA)). Data are reported as mean \pm SD (n = 3). Statistical analysis involved an analysis of variance using the Holm–Sidak method. **p < 0.001; *p < 0.05; n.s.d., no significant differences.

3.3.3 Behavior of HFF-1 and HaCaT cells

Several experiments and analysis were performed to study the behavior and interaction of HFF-1 and HaCaT cells with the ELR-click fibers. In a first experiment, 3000 cells/cm² of each type were seeded separately onto fiber mats with different fiber densities in order to evaluate the interaction between cells and fibers. As can be seen in Fig.7 (A, D, F and G), denser matrices offer more anchorage points for both kinds of cells, thus allowing good coverage of the

scaffolds by the cells. In contrast, a lower number of fibers allows a better view of the interaction of single cells with more isolated fibers (Fig 7 B, C, E, H and I).

Both types of cells developed their normal phenotype, as can be seen in fluorescence images (Fig.7) and histology pictures (Fig.8). The microscopy images in Fig 7 (B, C, H and I) show how HFF-1 attaches to randomly oriented isolated fibers and tends to follow the direction set by the fiber. Similarly, HaCaT cells attach to randomly oriented fibers at the edges of the patch-like structure that is usually formed, as can be seen in Fig. 7 (D, E and F).

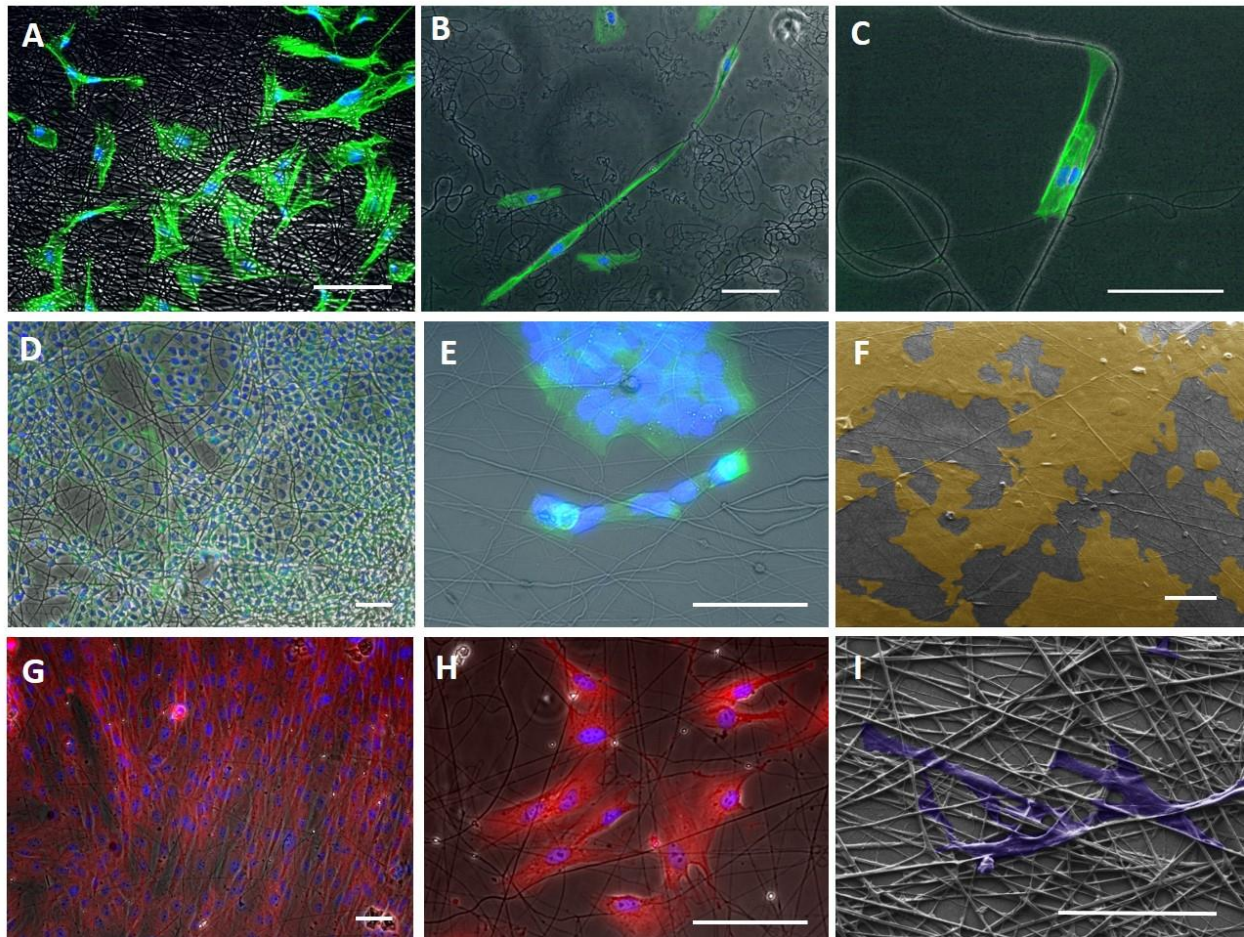


Fig. 7 Fluorescence microscopy with phalloidin (green) and DAPI (blue) staining of the cytoplasm and nucleus, respectively, in HFF-1 (A, B and C) and HaCaT cells (D and E) growing on randomly aligned fibers. Immunofluorescence staining with vinculin (red) and DAPI (blue) for the cytoplasm and nucleus, respectively, in HFF-1 cells (G and H). SEM images for HaCaT and HFF-1 cells (F and I, respectively). Cells were colored using Corel Paintshop Pro software (HFF-1 in blue and HaCaT cells in brown) for better observation. Scale bars: 50 μ m

Histology images and H/E and elastin staining (Fig. 8) showed that HaCaT cells grow in patch-like or mosaic-like structures rather than exhibiting an elongated morphology. The borders of these patches show how cells touch the

fibers and attach to them (Fig 8 D, E and F). Fig. 8 I shows a single HaCaT cell nicely attached to stained ELR-click fibers. H/E staining images (Fig. 8 A, B, C) highlight the different behavior of HFF-1 and HaCaT cells on the ELR-click fibers. Thus, whereas HFF-1 grows more independently until finally reaching confluence, HaCaT cells grow in separate clusters in which confluent cells multiply, thus allowing the cluster to grow.

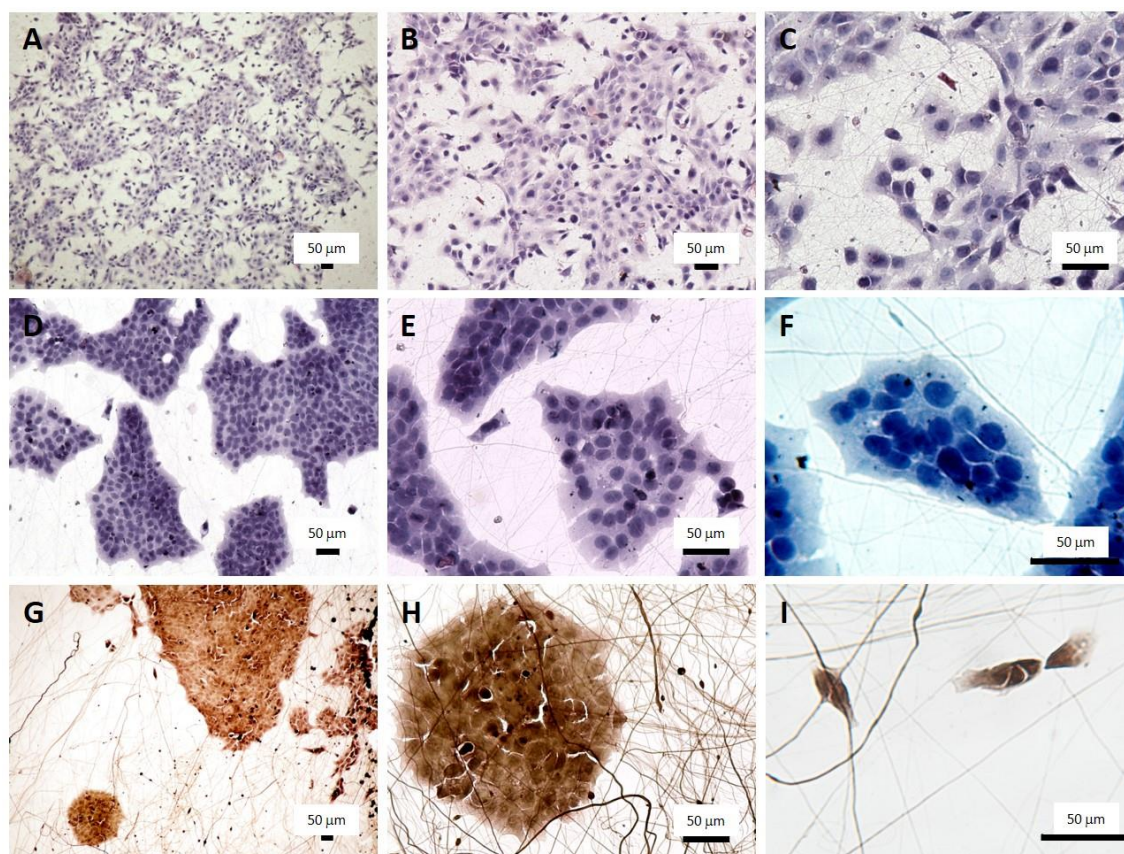
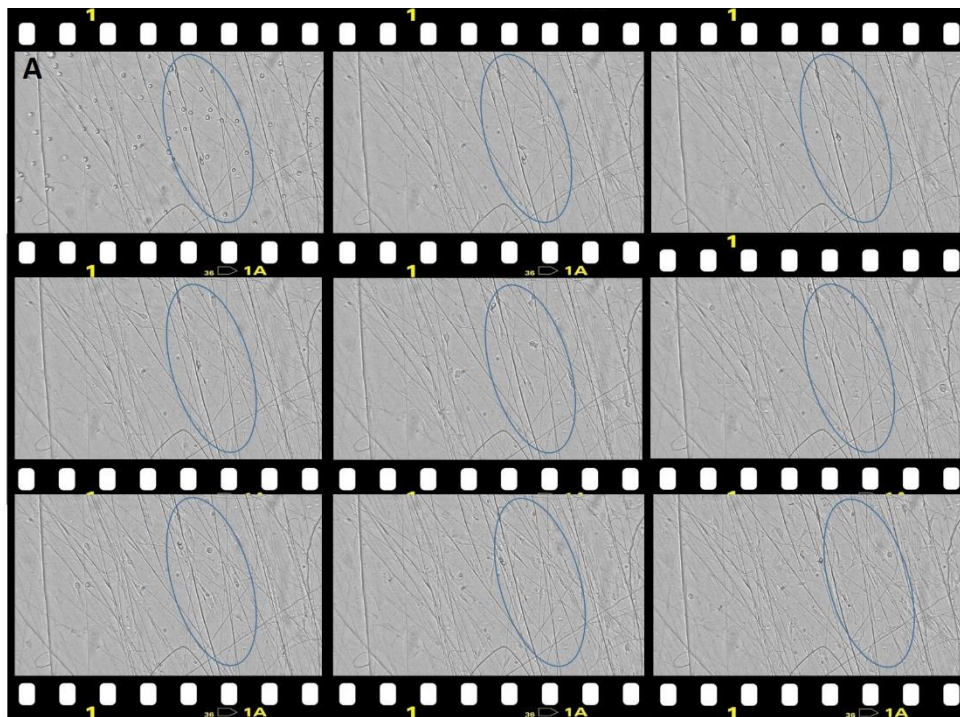


Fig. 8 H/E staining of HFF-1 (A, B and C) and HaCaT cells (D, E and F). Elastin staining of HaCaT cells (G, H and I), all at different magnifications. Scale bars: 50 µm

The growth of these two types of cells on ELR-click fibers was recorded over 48 hours. (See videos in supporting information). The sequences in Fig. 9 A and B depict the behavior of HFF-1 and HaCaT cells, respectively. Unfortunately, it is difficult to get a clear idea of how these two cell lines behave when they come into contact with ELR-click fibers from the sequences in Fig. 9, mainly due to the fact that we can only show a few snapshots from the full video. A better idea of the movements of these two cell lines can be obtained from the videos in the supporting information. HFF-1 attaches to the surfaces and fibers but elongates along the direction established by the ELR-click fibers. It is easy to see the microspikes expanding into the surrounding area until a fiber is finally

found. Once attached, the filopodia continue to explore the fiber or the vicinity, anchoring to another fiber and spreading the cytoplasm, even stretching up to 75 μm . Fibroblasts grow larger (from approximately 12 μm at the beginning of the culture to about 100 μm when they are completely spread) and colonize the area, but with no major displacements. Isolated HaCaT cells attach to the fibers and start to move along them, travelling relatively long distances until another cell is contacted or the distance from the starting point is too long, at which point they tend to divide and continue colonizing the area. In fact, a closer look at the movement of these cells shows how they leave a series of “waymarks” along the pathway that they have followed, thus allowing them to retrace their steps. The marked areas in Fig 9 A and B are an attempt to represent our observations and the explanation above.



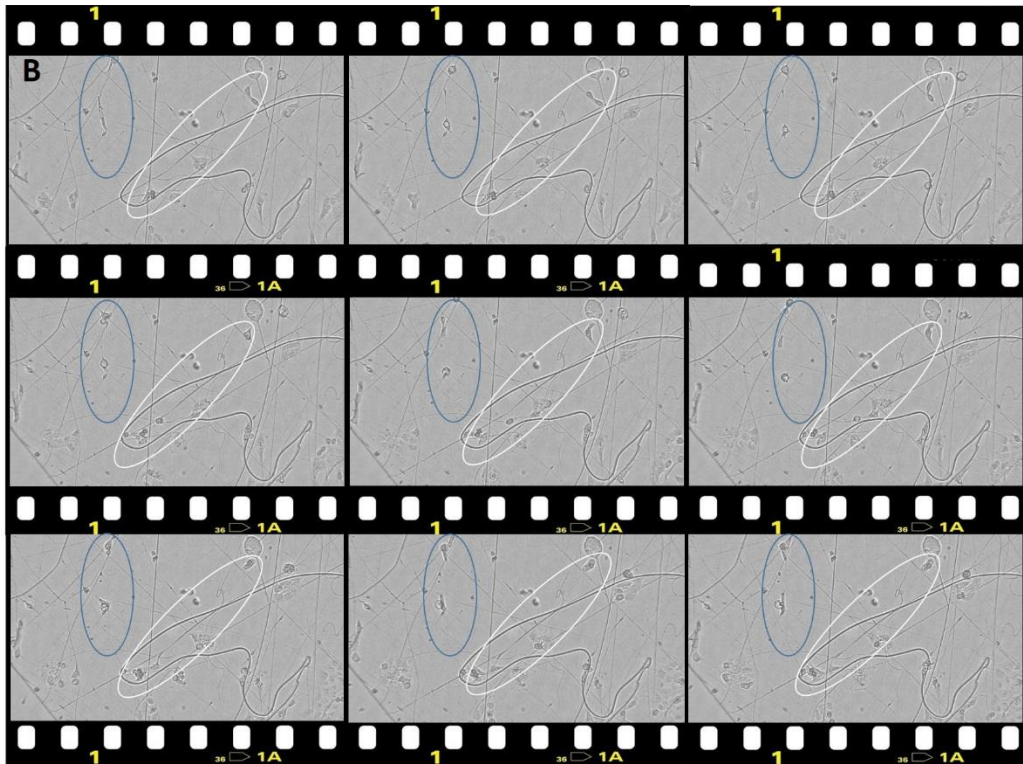


Fig. 9 Representative sequences for HFF-1 and HaCaT cells growing on random ELR-click fibers (A and B respectively) taken from videos recorded over 48 hours. See the supporting information for further details.

In the case of oriented ELR-click fibers, HFF-1 grew aligned to the fibers, as can be seen in Fig. 10 and in video 3 in the supporting information. In the initial stages, the cells attached to the surfaces and started to explore the surrounding area, interacting with ELR-click fibers and spreading their cytoplasm following the direction set by the ELR-click fibers. This behavior is not shared by HaCaT cells, which attach to and interact with the fibers but do not elongate following a clear direction (data not shown). This type of cell tends to form the classical patch-like structure mentioned above, colonizing the fibrous scaffold in random directions irrespective of the orientation of the fibers. The diameter of these patch-like structures grows from around 25 μm at the beginning of the culture to about 51 μm after 40 hours, as a consequence of cell proliferation.

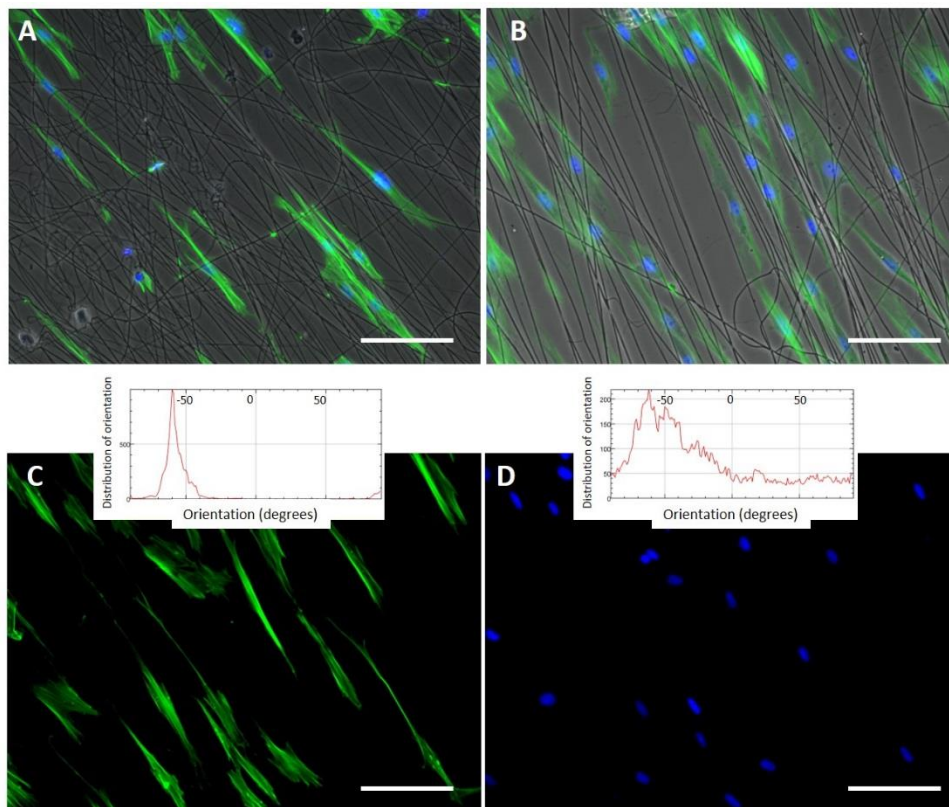


Fig. 10 Phalloidin and DAPI staining (green (cytoplasm) and blue (nucleus)) of oriented HFF-1 cells on ELR-click fibers. All channels are merged in A and B, whereas images C and D show the green and blue channels for cytoplasm and nucleus staining, respectively, for a better visualization of the extended morphology of the aligned HFF-1 cells. The inserts represent the orientation data for the cytoplasm and nucleus respectively. Scale bars: 50 μm

4 Discussion

Electrospinning has been shown to be a particularly useful technique for creating nano- and microfibers from a wide variety of materials over the past few years. Herein we describe the fabrication of ELR microfibers with dimensions (width of $1.11 \pm 0.45 \mu\text{m}$) that perfectly fit the values reported in the literature for fibers used for biomedical applications [55]. Both the formation of ELR fibers, a topic that has already been explored [56, 57], and the formation of stable fibers from two different ELRs has been achieved in this work. Our ELR-click fibers are obtained in a single-step process, with no need for any further crosslinking or fiber stabilization after the electrospinning process, by taking advantage of click chemistry, which allows us to crosslink functionalized ELRs in a rapid manner [41]. This is a clear step forward as it does away with the need for the crosslinking steps involving the use of toxic substances needed to stabilize fibers produced using other biomaterials [54, 58-63]. Indeed, this

multicomponent system permits the formation of fibers from a combination of at least two ELRs with different bioactivities in a single process.

Several conditions were explored to create the ELR-click fibers and the optimized values found to be similar to the optimal conditions found in the literature [25] (mainly a voltage of 18k V, 298 K, humidity of 35%, distance between electrodes of 9 cm) for the production of this kind of fiber. However, one clear difference with respect to other electrospun fibers is the solution concentration (50 mg/mL), which in the ELR-click fiber is lower than the concentration used for the formation of fibers from other materials [23-25]. We suggest that this difference is due to the fact that our two-component system is able to form gels by itself, in a very short time, at this concentration [41, 45]. During this electrospinning process, the click reaction takes place from the very moment that both components come together inside the needle on their way to the collector. The solvent is evaporated during this short time and the gel formed at the tip of the needle is stretched until a fiber is formed. The ribbon-like and wrinkled surface of the ELR-click fibers have already been described for other kinds of electrospun fibers[64, 65] and have been associated to a deformation mismatch between the shell and the core of the fiber during solvent evaporation, thereby resulting in a wrinkled topography [65]. Very high contact angle values for long deposition times ($>100^\circ$) indicate a marked hydrophobicity for the scaffolds. In fact, it has been suggested [65] that the hydrophobic behavior of non-woven mats is enhanced because wrinkling.

Furthermore, the purpose of a scaffold is not only to provide a surface for cell attachment and spreading, but also to have mechanical stability at the defect site. Thus, a well-designed tissue engineered scaffold must provide sufficient biomechanical support during the regeneration process. Here, the average ultimate tensile strength values obtained for our scaffolds (0.59 ± 0.08 MPa) agree with the ones found in the literature for fibers made of elastin or blends of elastin and other materials [66-69]. It is important to note that the purpose of these scaffolds is not to substitute the mature skin, but to improve skin regeneration in order to get a mature tissue.

Although Weiss and co-workers have explored the possibility of using tropoelastin-based materials for skin-tissue engineering applications over the last decade, [54, 60], genetically engineered elastin-like polymers have not yet been processed as fibers for use in skin regeneration. In this work, keratinocytes (HaCaT cells) and fibroblasts (HFF-1), which are two of the main cell populations in the epidermis and dermis, respectively, were seeded on ELR-

click fibers and found to exhibit excellent adhesion and proliferation profiles, similar to those for the positive controls.

In low density matrices, fluorescence microscopy showed the affinity of both types of cells for the ELR-click fibers and the spontaneous trend to follow their direction (Fig. 7). This behavior is mainly observed in fibroblast cultures (Fig 7 B and C) due to their inherent elongated morphology, which allows them to follow the pathway marked by the RGD-containing fibers. This trend was corroborated by the behavior of the cells recorded during culture for 48 hours. Clear differences between both cell types can be seen in the video sequences (see supporting information). Thus, keratinocytes actively migrate along the fibers then finally retrace their steps and split into two cells. This was repeatedly observed until a classical mosaic-like structure was formed. Fibroblasts, in contrast, tend to attach to the fibers and elongate their cytoplasm following the pathway marked by the fibers or until they find a nearby fiber to attach to, as can be seen in fluorescence images in Fig. 7B and 7C. This behavior was not so evident at higher fiber densities due to the large number of points that a dense matrix offers to the cells to attach isotropically instead of following the path of a single fiber.

Histological evaluation by hematoxylin-eosin (H/E) staining (Fig. 8) corroborated this behavior for keratinocytes, which first attached to and followed the fibers then rapidly started to spread out, finally adopting the tile morphology that will form part of a larger mosaic of cells. However, the preference of keratinocytes for ELR click-fibers is clear even in these patch or mosaic-like structures, as can be seen from the cells at the borders of the mosaic-like structure. This preference for the ELR-click fibers is clearly visible in the elastin staining histology images (Fig. 8 G, H and I), where the fibers are clearly stained and the cells at the borders of the mosaic unmistakably elongate to attach to the closest fiber. The vinculin fluorescence immunostaining images show the cells attached to the fibers, along with some bright red dots where this attachment is actively being established with the fiber.

In addition to randomly oriented stable fibers, we also obtained aligned fibers with a coherency of more than 80% by way of a careful process in which the speed at the surface of a rotatory mandrel had to be adjusted to the speed of the fiber projected from the tip of the needle. Lower than optimal rotation speeds lead to non-aligned fibers, whereas a faster rotation speed leads to very thin and fragmented fibers. This speed at the surface of the rotatory mandrel was adjusted to 1.8 m/s under the same fixed electrospinning conditions used to obtain non-aligned fibers. In this case, fibroblasts visibly grow aligned with the fiber direction, as can be seen from the fluorescence images of actin-

stained cells. This alignment involves both a cytoskeletal orientation and a nuclear alignment, as can be seen from the green and blue channel images after phalloidin and DAPI staining, respectively (Fig. 10 C and D). This behavior has also been observed in other kinds of cells (human stem cells and neural stem cells) attached to poly ϵ -caprolactone [28, 70] and poly(l-lactide) fibers [71].

Wound dressings for skin tissue engineering are one of the many applications in which electrospun scaffolds have been used. These artificial scaffolds usually lack the desired elasticity after implantation, mainly due to two factors, namely that electrospun fibers are made of non-elastic materials and the low elastin production and secretion by cells during the regeneration process [72-75]. The aforementioned lack of elastin and the overproduction of collagen fibers by fibroblasts and keratinocytes is one of the main issues responsible for the shrinkage of artificial skin scaffolds. Therefore, the presence of elastin derivatives, such as the ELRs, might theoretically prevent this shrinking, giving a better handling of the scaffold and providing the native elasticity to the artificial skin.

Consequently, a system that could induce the growth of keratinocytes and fibroblasts on random or aligned ELR-fibers is a very interesting approach to create scaffolds that promote regeneration of the skin after serious injuries by mimicking the elasticity and biological properties of this tissue. H/E and elastin staining highlighted the normal growth and behavior of the two different cell lines, both of which developed their normal phenotype. Thus, HFF-1 grew by spreading its cytoplasm and multiplying until confluence was reached, whereas HaCaT cells grew to form patch-like clusters that grew until a confluent layer had been obtained. Complete layers of fibroblasts and keratinocytes were obtained on top of dense ELR-click fiber matrixes, thus highlighting the suitability of these scaffolds for skin tissue engineering applications.

5 Conclusions

Electrospun fibers usually need a post-treatment to stabilize them. However, many of the crosslinking methods proposed for that purpose make use of solvents or organic compounds that are harmful to cells and therefore have to be removed prior to the subsequent use of these fibers in cell culture. Moreover, the electrospun ELR fibers reported to date need further treatment to be stable in water solutions. Herein we have presented a system for obtaining fibers from clickable ELRs that crosslink during the flight of the fiber from the tip of the needle to the collector electrode. These ELR-click fibers do not need any further stabilization treatment and are completely stable under *in vitro*

conditions. To the best of our knowledge, there are no reports in the literature of bi-component fibers that do not need further crosslinking after the electrospinning process. A wrinkled fiber morphology was observed in the SEM images, and both random and oriented fiber orientations, with a high degree of alignment and coherence, have been produced making use of a rotational electrode. Moreover, these ELR-click fibers open up the possibility of incorporate different functionalities into each ELR that will contribute to the final overall fiber functionality.

The cytocompatibility of these ELR-click fibers has been clearly proved by way of adhesion and proliferation studies during *in vitro* experiments in which the growth of keratinocytes and fibroblasts, the two main cell lines found in the dermis and epidermis, on the ELR-click fibers is similar and follows the same trend as for the positive controls. The affinity of these two cell lines for the ELR-click fibers has also been proven, as can be seen from the videos recorded for both cell types during culture. Optical fluorescence images and a histological analysis of the growth of these two cell lines indicate the possibility of using scaffolds based on ELR-click fibers for wound dressings in skin tissue engineering applications. Finally, we have describe the preparation of electrospun scaffolds that can be used directly after the electrospinning process as wound dressing to cover skin damaged areas or alternatively they can be *in vitro* colonized by skin cell lines to prepare an artificial skin substitute that could be implanted in the wounded area.

Acknowledgements

This study was funded by the European Commission (ELASTISLET No 646075, BIOGEL No 642687), the Ministerio de Economía y Competitividad of the Spanish Government (MAT2015-68901-R, MAT2016-78903-R, PCIN-2015-010) and the Junta de Castilla y León (VA015U16).

REFERENCES

- [1] S.R. Caliari, J.A. Burdick, A practical guide to hydrogels for cell culture, *Nat Meth* 13(5) (2016) 405-414.
- [2] A. Prasad, M.R. Sankar, V. Katiyar, State of Art on Solvent Casting Particulate Leaching Method for Orthopedic ScaffoldsFabrication, *Materials today* 4 (2017) 898-907.
- [3] D.B. Hall, P. Underhill, J.M. Torkelson, Spin coating of thin and ultrathin polymer films, *Polymer Engineering & Science* 38(12) (1998) 2039-2045.
- [4] X. Zong, H. Bien, C.Y. Chung, L. Yin, D. Fang, H.-B.S. Biomaterials, Electrospun fine-textured scaffolds for heart tissue constructs, *Biomaterials* 26(26) (2005) 5330-8.
- [5] M. Saini, Y. Singh, P. Arora, V. Arora, K. Jain, Implant biomaterials: A comprehensive review, *World Journal of Clinical Cases* : WJCC 3(1) (2015) 52-57.

- [6] E.S. Place, N.D. Evans, M.M. Stevens, Complexity in biomaterials for tissue engineering, *Nat Mater* 8(6) (2009) 457-470.
- [7] J. Scheib, A. Höke, *Advances in peripheral nerve regeneration*, 9 (2013) 668.
- [8] N.J. Schaub, C.D. Johnson, B. Cooper, R.J. Gilbert, Electrospun Fibers for Spinal Cord Injury Research and Regeneration, *Journal of Neurotrauma* 33(15) (2016) 1405-1415.
- [9] C.K. Kuo, J.E. Marturano, R.S. Tuan, Novel strategies in tendon and ligament tissue engineering: Advanced biomaterials and regeneration motifs, *Sports Medicine, Arthroscopy, Rehabilitation, Therapy & Technology: SMARTT 2* (2010) 20-20.
- [10] N. Sevivas, G. França, N. Oliveira, H. Pereira, K.W. Ng, A. Salgado, J. Espregueira-Mendes, Biomaterials for Tendon Regeneration, in: G.L. Canata, P. d'Hooghe, K.J. Hunt (Eds.), *Muscle and Tendon Injuries: Evaluation and Management*, Springer Berlin Heidelberg, Berlin, Heidelberg, 2017, pp. 131-143.
- [11] B.J. Kwee, D.J. Mooney, Biomaterials for skeletal muscle tissue engineering, *Current Opinion in Biotechnology* 47(Supplement C) (2017) 16-22.
- [12] T.H. Qazi, D.J. Mooney, M. Pumberger, S. Geißler, G.N. Duda, Biomaterials based strategies for skeletal muscle tissue engineering: Existing technologies and future trends, *Biomaterials* 53(Supplement C) (2015) 502-521.
- [13] M.M. Stevens, Biomaterials for bone tissue engineering, *Materials Today* 11(5) (2008) 18-25.
- [14] X. Yu, X. Tang, S.V. Gohil, C.T. Laurencin, Biomaterials for Bone Regenerative Engineering, *Adv Healthc Mater* 4(9) (2015) 1268-85.
- [15] S. MacNeil, Biomaterials for tissue engineering of skin, *Materials today* 11(5) (2008) 26-35.
- [16] A.D. Metcalfe, M.W.J. Ferguson, Tissue engineering of replacement skin: the crossroads of biomaterials, wound healing, embryonic development, stem cells and regeneration, *Journal of the Royal Society Interface* 4(14) (2007) 413-437.
- [17] A.A. Chaudhari, K. Vig, D.R. Baganizi, R. Sahu, S. Dixit, V. Dennis, S.R. Singh, S.R. Pillai, Future Prospects for Scaffolding Methods and Biomaterials in Skin Tissue Engineering: A Review, *International Journal of Molecular Sciences* 17(12) (2016) 1974.
- [18] E. Proksch, J.M. Brandner, J.M. Jensen, The skin: an indispensable barrier, *Experimental dermatology* 17(12) (2008) 1063-72.
- [19] S.F. Gilbert, *Developmental Biology*, 6th edition, Sunderland (MA): Sinauer Associates 2000.
- [20] B. Vrhovski, A.S. Weiss, Biochemistry of tropoelastin, *Eur J Biochem* 258(1) (1998) 1-18.
- [21] J.F. Almine, S.G. Wise, A.S. Weiss, Elastin signaling in wound repair, *Birth Defects Research Part C: Embryo Today: Reviews* 96(3) (2012) 248-257.
- [22] G. Broughton, 2nd, J.E. Janis, C.E. Attinger, The basic science of wound healing, *Plast Reconstr Surg* 117(7 Suppl) (2006) 12s-34s.
- [23] M. Li, M.J. Mondrinos, M.R. Gandhi, F.K. Ko, A.S. Weiss, P.I. Leikes, Electrospun protein fibers as matrices for tissue engineering, *Biomaterials* 26(30) (2005) 5999-6008.
- [24] D. Han, P.-I. Gouma, Electrospun bioscaffolds that mimic the topology of extracellular matrix, *Nanomedicine: Nanotechnology, Biology and Medicine* 2(1) (2006) 37-41.
- [25] A. Greiner, J.H. Wendorff, Electrospinning: a fascinating method for the preparation of ultrathin fibers, *Angew Chem Int Ed Engl* 46(30) (2007) 5670-703.
- [26] S.A. Sell, M.J. McClure, K. Garg, P.S. Wolfe, Electrospinning of collagen/biopolymers for regenerative medicine and cardiovascular tissue engineering, *Advanced drug delivery ...* (2009).
- [27] D.B. Khadka, D.T. Haynie, Protein-and peptide-based electrospun nanofibers in medical biomaterials, *Nanomedicine: Nanotechnology, Biology and Medicine* 8(8) (2012) 1242-1262.
- [28] X. Wang, B. Ding, L.-B. today, Biomimetic electrospun nanofibrous structures for tissue engineering, *Materials today* 16(6) (2013) 229-241.

- [29] J.I. Kim, T.I. Hwang, L.E. Aguilar, C.H. Park, C.S. Kim, A Controlled Design of Aligned and Random Nanofibers for 3D Bi-functionalized Nerve Conduits Fabricated via a Novel Electrospinning Set-up, 6 (2016) 23761.
- [30] X. Li, M. Li, J. Sun, Y. Zhuang, J. Shi, D. Guan, C.-Y. Small, Radially Aligned Electrospun Fibers with Continuous Gradient of SDF1 α for the Guidance of Neural Stem Cells, Small (2016).
- [31] W. Wang, S. Itoh, K. Konno, T. Kikkawa, S. Ichinose, K. Sakai, T. Ohkuma, K. Watabe, Effects of Schwann cell alignment along the oriented electrospun chitosan nanofibers on nerve regeneration, J Biomed Mater Res A 91(4) (2009) 994-1005.
- [32] I.M. Braverman, E. Fonferko, Studies in Cutaneous Aging: I. The Elastic Fiber Network, Journal of Investigative Dermatology 78(5) (1982) 434-443.
- [33] J. Uitto, D.J. Santa Cruz, A.Z. Eisen, Connective tissue nevi of the skin: Clinical, genetic, and histopathologic classification of hamartomas of the collagen, elastin, and proteoglycan type, Journal of the American Academy of Dermatology 3(5) (1980) 441-461.
- [34] A.C. Weihermann, M. Lorencini, C.A. Brohem, C.M. de Carvalho, Elastin structure and its involvement in skin photoageing, International Journal of Cosmetic Science 39 (2017) 241-247.
- [35] J. Dallon, J. Sherratt, P. Maini, M. Ferguson, Biological implications of a discrete mathematical model for collagen deposition and alignment in dermal wound repair, Mathematical Medicine and Biology: A Journal of the IMA 17(4) (2000) 379-393.
- [36] A. Girotti, D. Orbanic, A. Ibáñez-Fonseca, C. Gonzalez-Obeso, J.C. Rodríguez-Cabello, Recombinant Technology in the Development of Materials and Systems for Soft-Tissue Repair, Advanced Healthcare Materials 4(16) (2015) 2423-2455.
- [37] J.C. Rodríguez-Cabello, L. Martín, M. Alonso, F.J. Arias, A.M. Testera, "Recombinamers" as advanced materials for the post-oil age, Polymer 50(22) (2009) 5159-5169.
- [38] D.W. Urry, What Sustains Life? Consilient Mechanisms for Protein-Based Machines and Materials, Birkhäuser Boston, Boston (USA), 2006.
- [39] D.W. Urry, Molecular Machines - How Motion and Other Functions of Living Organisms Can Result from Reversible Chemical-Changes, Angewandte Chemie (International ed. in English) 32(6) (1993) 819-841.
- [40] I. González de Torre, L. Quintanilla, G. Pinedo-Martín, M. Alonso, J.C. Rodríguez-Cabello, Nanogel Formation from Dilute Solutions of Clickable Elastin-like Recombinamers and its Dependence on Temperature: Two Fractal Gelation Modes, ACS Applied Materials & Interfaces 6(16) (2014) 14509-14515.
- [41] I. González de Torre, M. Santos, L. Quintanilla, A. Testera, M. Alonso, J.C. Rodríguez Cabello, Elastin-like recombinamer catalyst-free click gels: Characterization of poroelastic and intrinsic viscoelastic properties, Acta Biomaterialia 10(6) (2014) 2495-2505.
- [42] L. Debelle, A.M. Tamburro, Elastin: molecular description and function, International Journal of Biochemistry & Cell Biology 31(2) (1999) 261-272.
- [43] P. Brown-Augsburger, C. Tisdale, T. Broekelmann, C. Sloan, R.P. Mecham, Identification of an elastin cross-linking domain that joins three peptide chains possible role in nucleated assembly, Journal of Biological Chemistry 270(30) (1995) 17778-17783.
- [44] S.M. Staubli, G. Cerino, I. Gonzalez De Torre, M. Alonso, D. Oertli, F. Eckstein, K. Glatz, J.C. Rodríguez Cabello, A. Marsano, Control of angiogenesis and host response by modulating the cell adhesion properties of an Elastin-Like Recombinamer-based hydrogel, Biomaterials 135 (2017) 30-41.
- [45] I. González de Torre, F. Wolf, M. Santos, L. Rongen, M. Alonso, S. Jockenhoevel, J.C. Rodríguez-Cabello, P. Mela, Elastin-like recombinamer-covered stents: Towards a fully biocompatible and non-thrombogenic device for cardiovascular diseases, Acta Biomaterialia 12(0) (2015) 146-155.
- [46] E. Ruoslahti, M.D. Pierschbacher, Arg-Gly-Asp: A versatile cell recognition signal, Cell 44(4) (1986) 517-518.

- [47] A. Ibáñez-Fonseca, T.L. Ramos, I.G. de Torre, L.I. Sánchez-Abarca, S. Muntión, F.J. Arias, M.C. del Cañizo, M. Alonso, F. Sánchez-Guijo, J.C. Rodríguez-Cabello, Biocompatibility of two model elastin-like recombinamer-based hydrogels formed through physical or chemical crosslinking for various applications in tissue engineering and regenerative medicine, *Journal of Tissue Engineering and Regenerative Medicine* 2017 1-11.
- [48] Z. Puspoki, M. Storath, D. Sage, M. Unser, *Transforms and Operators for Directional Bioimage Analysis: A Survey*, *Advances in anatomy, embryology, and cell biology* 219 (2016) 69-93.
- [49] E. Fonck, G.G. Feigl, J. Fasel, D. Sage, M. Unser, D.A. Rüfenacht, N. Stergiopoulos, Effect of Aging on Elastin Functionality in Human Cerebral Arteries, *Stroke* 40(7) (2009) 2552-2556.
- [50] R. Rezakhaniha, A. Agianniotis, J.T. Schrauwen, A. Griffa, D. Sage, C.V. Bouten, F.N. van de Vosse, M. Unser, N. Stergiopoulos, Experimental investigation of collagen waviness and orientation in the arterial adventitia using confocal laser scanning microscopy, *Biomechanics and modeling in mechanobiology* 11(3-4) (2012) 461-73.
- [51] R. Rezakhaniha, A. Agianniotis, J.T.C. Schrauwen, A. Griffa, D. Sage, C.V.C. Bouten, F.N. van de Vosse, M. Unser, N. Stergiopoulos, Experimental investigation of collagen waviness and orientation in the arterial adventitia using confocal laser scanning microscopy, *Biomechanics and modeling in mechanobiology* 11(3) (2012) 461-473.
- [52] R. Machado, A. da Costa, V. Sencadas, C. Garcia-Arévalo, C.M. Costa, J. Padrão, A. Gomes, S. Lanceros-Méndez, J. Rodríguez-Cabello, M. Casal, Electrospun silk-elastin-like fibre mats for tissue engineering applications, *Biomedical Materials* 8(6) (2013) 1-13.
- [53] L. Buttafoco, N.G. Kolkman, P. Engbers-Buijtenhuijs, A.A. Poot, P.J. Dijkstra, I. Vermes, J. Feijen, Electrospinning of collagen and elastin for tissue engineering applications, *Biomaterials* 27(5) (2006) 724-734.
- [54] L. Nivison-Smith, J. Rnjak, A.S. Weiss, Synthetic human elastin microfibers: stable cross-linked tropoelastin and cell interactive constructs for tissue engineering applications, *Acta biomaterialia* 6(2) (2010) 354-359.
- [55] C.P. Barnes, S.A. Sell, E.D. Boland, D.G. Simpson, G.L. Bowlin, Nanofiber technology: Designing the next generation of tissue engineering scaffolds, *Advanced Drug Delivery Reviews* 59(14) (2007) 1413-1433.
- [56] M. Putzu, F. Causa, V. Nele, I.G. de Torre, Elastin-like-recombinamers multilayered nanofibrous scaffolds for cardiovascular applications, *Biofabrication* 8(4) (2016) 1-14.
- [57] L. Huang, R.A. McMillan, R.P. Apkarian, B. Pourdeyhimi, V.P. Conticello, E.L. Chaikof, Generation of Synthetic Elastin-Mimetic Small Diameter Fibers and Fiber Networks, *Macromolecules* 33(8) (2000) 2989-2997.
- [58] J. Rnjak-Kovacina, S.G. Wise, Z. Li, P.K. Maitz, C.J. Young, Y. Wang, A.S. Weiss, Tailoring the porosity and pore size of electrospun synthetic human elastin scaffolds for dermal tissue engineering, *Biomaterials* 32(28) (2011) 6729-36.
- [59] J. Rnjak-Kovacina, S.G. Wise, Z. Li, P.K. Maitz, C.J. Young, Y. Wang, A.S. Weiss, Electrospun synthetic human elastin:collagen composite scaffolds for dermal tissue engineering, *Acta biomaterialia* 8(10) (2012) 3714-3722.
- [60] L. Nivison-Smith, A.S. Weiss, Alignment of human vascular smooth muscle cells on parallel electrospun synthetic elastin fibers, *J Biomed Mater Res A* 100(1) (2011) 155-61.
- [61] Y. Ner, J.A. Stuart, G. Whited, G.A. Sotzing, Electrospinning nanoribbons of a bioengineered silk-elastin-like protein (SELP) from water, *Polymer* (2009).
- [62] Z.G. Chen, P.W. Wang, B. Wei, X.M. Mo, F.Z. Cui, Electrospun collagen-chitosan nanofiber: A biomimetic extracellular matrix for endothelial cell and smooth muscle cell, *Acta Biomaterialia* 6(2) (2010) 372-382.

- [63] P.L. Benitez, J.A. Sweet, H. Fink, K.P. Chennazhi, S.V. Nair, A. Enejder, S.C. Heilshorn, Sequence-Specific Crosslinking of Electrospun, Elastin-Like Protein Preserves Bioactivity and Native-Like Mechanics, *Advanced Healthcare Materials* 2(1) (2013) 114-118.
- [64] S. Koombhongse, W. Liu, D.H. Reneker, Flat polymer ribbons and other shapes by electrospinning, *Journal of Polymer Science Part B: Polymer Physics* 39(21) (2001) 2598-2606.
- [65] L. Wang, C.L. Pai, M.C. Boyce, R.-G.C. Letters, Wrinkled surface topographies of electrospun polymer fibers, *Applied Physics Letters* (2009).
- [66] M. Li, M.J. Mondrinos, X. Chen, M.R. Gandhi, F.K. Ko, P.I. Leikes, Co-electrospun poly(lactide-co-glycolide), gelatin, and elastin blends for tissue engineering scaffolds, *J Biomed Mater Res A* 79(4) (2006) 963-73.
- [67] M.J. McClure, S.A. Sell, C.E. Ayres, D.G. Simpson, G.L. Bowlin, Electrospinning-aligned and random polydioxanone–polycaprolactone–silk fibroin-blended scaffolds: geometry for a vascular matrix, *Biomedical Materials* 4(5) (2009) 055010.
- [68] X. Zhang, V. Thomas, Y.K. Vohra, In vitro biodegradation of designed tubular scaffolds of electrospun protein/polyglyconate blend fibers, *J Biomed Mater Res B Appl Biomater* 89(1) (2009) 135-47.
- [69] E. Sayin, R.H. Rashid, J.C. Rodríguez-Cabello, A. Elsheikh, E.T. Baran, V. Hasirci, Human adipose derived stem cells are superior to human osteoblasts (HOB) in bone tissue engineering on a collagen-fibroin-ELR blend, *Bioactive Materials* 2(2) (2017) 71-81.
- [70] S.Y. Chew, R. Mi, A. Hoke, K.W. Leong, The Effect of the Alignment of Electrospun Fibrous Scaffolds on Schwann Cell Maturation, *Biomaterials* 29(6) (2008) 653-661.
- [71] L. He, S. Liao, D. Quan, K. Ma, C. Chan, S. Ramakrishna, J. Lu, Synergistic effects of electrospun PLLA fiber dimension and pattern on neonatal mouse cerebellum C17.2 stem cells, *Acta Biomaterialia* 6(8) (2010) 2960-2969.
- [72] F.A. Auger, M. Rouabhia, F. Goulet, F. Berthod, V. Moulin, L. Germain, Tissue-engineered human skin substitutes developed from collagen-populated hydrated gels: clinical and fundamental applications, *Med Biol Eng Comput* 36(6) (1998) 801-12.
- [73] I. Ono, T. Tateshita, M. Inoue, Effects of a collagen matrix containing basic fibroblast growth factor on wound contraction, *J Biomed Mater Res* 48(5) (1999) 621-30.
- [74] D.P. Berry, K.G. Harding, M.R. Stanton, B. Jasani, H.P. Ehrlich, Human wound contraction: collagen organization, fibroblasts, and myofibroblasts, *Plast Reconstr Surg* 102(1) (1998) 124-31; discussion 132-4.
- [75] H.M. Powell, S.T. Boyce, Engineered human skin fabricated using electrospun collagen-PCL blends: morphogenesis and mechanical properties, *Tissue Eng Part A* 15(8) (2009) 2177-87.